



Research papers

Ensemble-based flood vulnerability assessment for probable maximum flood in a changing environment[☆]



Sudershan Gangrade^{a,b,c}, Shih-Chieh Kao^{a,b,c,*}, Tigstu T. Dullo^d, Alfred J. Kalyanapu^d, Benjamin L. Preston^e

^a The Bredeben Center, University of Tennessee, Knoxville, TN 37996, USA

^b Environmental Sciences Division, Oak Ridge National Laboratory, Oak Ridge, TN 37831, USA

^c Climate Change Science Institute, Oak Ridge National Laboratory, Oak Ridge, TN 37831, USA

^d Department of Civil and Environmental Engineering, Tennessee Technological University, Cookeville, TN 38505, USA

^e RAND Corporation, P.O. Box 2138, Santa Monica, CA 90407, USA

ARTICLE INFO

This manuscript was handled by Emmanouil Anagnostou, Editor-in-Chief

Keywords:

Flood modeling

Graphics Processing Units (GPU)

Probable maximum precipitation (PMP)

Probable maximum flood (PMF)

Probabilistic flood maps (PFMs)

ABSTRACT

The magnitude and frequency of hydro-meteorological extremes are expected to increase in a changing environment in ways that threaten the security of US energy-water assets. These include probable maximum precipitation (PMP) and probable maximum flood (PMF), which are used as hydraulic design standards for highly sensitive infrastructures such as nuclear power plants and main dams. To assess the flood vulnerability due to PMP/PMF, an integrated high-resolution process-based hydro-meteorologic modeling framework was used to develop ensemble-based probabilistic flood maps based on best-available historic observations and future climate projections. A graphics processing unit-accelerated 2-dimensional hydrodynamic model was used to simulate the surface inundation areas corresponding to a total of 120 PMF hydrographs. These ensemble-based PMF maps were compared with flood maps obtained from the conventional deterministic PMP/PMF approach, revealing added information about conditional probability of flooding. Further, a relative sensitivity test was conducted to explore the effects of various factors in the framework, such as meteorological forcings, antecedent hydrologic conditions, reservoir storage, and flood model input resolution and parameters. The proposed framework better illustrates the uncertainties associated with model inputs, parameterization, and hydro-meteorological factors, allowing more informed decision-making for future emergency preparation.

1. Introduction

Floods are one of the most destructive natural hazards, causing mortality, property loss, and infrastructure damage worldwide. The United States (US) alone has observed 29 billion-dollar-scale flood events in the period of 1980–2018 with a total of 543 deaths and roughly 122 billion dollars in inflation-adjusted losses (NCEI, 2018). The increasing frequency and magnitude of flood events under changing climate, population, and land use and land cover conditions require better predictability and preparedness for flood hazards. Flood inundation maps serve as a critical input to flood risk assessments and enable the development of informed floodplain management and mitigation strategies. In the US, the Federal Emergency Management

Agency (FEMA) utilizes hydrologic and hydraulic models to delineate flood inundation zones associated with 1% and 0.2% annual exceedance probability (AEP) (or 100-year and 500-year return periods) to support the National Flood Insurance Program (FEMA, 2018). For critical energy-water infrastructures, including major hydropower dams and nuclear power plants, even rarer events (AEP < 0.2%) or probable maximum flood (PMF) are the focus. Similar inundation maps developed for PMF-scale events may serve as useful tools to evaluate the vulnerability of critical infrastructures under worst-case flooding scenarios, as well as to identify regions with minimum flooding likelihood to support future site selection.

A general procedure to prepare flood inundation maps (hereinafter referred as a “modeling chain”) associated with PMF involves probable

[☆] Notice: This manuscript has been authored by UT-Battelle, LLC, under contract DE-AC05-00OR22725 with the US Department of Energy (DOE). The US government retains and the publisher, by accepting the article for publication, acknowledges that the US government retains a nonexclusive, paid-up, irrevocable, worldwide license to publish or reproduce the published form of this manuscript, or allow others to do so, for US government purposes. DOE will provide public access to these results of federally sponsored research in accordance with the DOE Public Access Plan (<http://energy.gov/downloads/doe-public-access-plan>).

* Corresponding author at: P.O. Box 2008, MS-6038, Oak Ridge, TN 37831-6038, USA.

E-mail address: kaos@ornl.gov (S.-C. Kao).

maximum precipitation (PMP) estimation, followed by hydrologic simulation and hydrodynamic/hydraulic modeling. Since the current practice of PMP/PMF assessment focuses on estimating the single deterministic maximum precipitation and streamflow event (that could occur under a series of adverse hydro-meteorological conditions), conventional PMF inundation maps are also deterministic in nature. However, deterministic maps inevitably mask out underlying uncertainties from decision makers or planners, given the binary (wet or dry) representation of the resulting flood inundation maps. While advanced deterministic maps employ process-based hydrologic and hydraulic models calibrated to historic events (Di Baldassarre et al., 2010), these maps are unable to capture the uncertainties arising from various other sources in the modeling chain, such as inaccurate input data, boundary conditions, model structure, and model parameterization (Alfonso et al., 2016; Di Baldassarre et al., 2010). Therefore, the value and potential of probabilistic flood maps (PFMs) have been highlighted recently in the literature (Alfonso et al., 2016; Di Baldassarre et al., 2010; Papaioannou et al., 2017). Recent advances in computational power have allowed the use of computationally intensive hydrologic-hydraulic models to develop PFMs through multi-ensemble simulation (Neal et al., 2013). The uncertainty characterization may be performed at various stages of the modeling chain by varying factors such as precipitation (Caseri et al., 2016), spatio-temporal rainfall variability (Jenkins et al., 2017; Nuswantoro et al., 2016; Zischg et al., 2018), spatial dependence of flow from tributaries (Neal et al., 2013; Pattison et al., 2014), hydrologic model parameters or inputs (Domeneghetti et al., 2013), hydraulic model types (Papaioannou et al., 2016), hydraulic model roughness coefficient (Papaioannou et al., 2017), and different digital elevation models and observational data sets (Giustarini et al., 2016; Papaioannou et al., 2016).

Although a few studies have focused on the development of flood inundation maps for the largest historic events (e.g., Pedrozo-Acuña et al., 2015) or for events with return periods ranging from hundreds (Smemoe et al., 2007; Kalyanapu et al., 2012) to thousands of years (Büchele et al., 2006; Prime et al., 2016), studies evaluating flood inundation maps for rare hydroclimatic extreme events such as PMP/PMF are limited (Zischg et al., 2018). Further, recent studies have suggested that PMP/PMF are sensitive to the changing climatic conditions (e.g., Kunkel et al., 2013; Beauchamp et al., 2013; Rousseau et al., 2014; Stratz and Hossain, 2014; Klein et al., 2016; Rastogi et al., 2017; Gangrade et al., 2018) and challenged the deterministic treatment of PMP/PMF. It has also been suggested that both epistemic and aleatoric uncertainties are involved in the estimation of PMP (Micovic et al., 2015). For instance, PMP and PMF estimates are often derived for a point location of interest without considering variability originating from spatiotemporal rainfall distribution or watershed heterogeneity. Through Monte Carlo simulation, Zischg et al. (2018) demonstrated that the spatiotemporal distribution of PMP has significant effects on the resulting PMF inundation maps. Other factors such as meteorological forcings, antecedent soil moisture, land-use land-cover conditions, and reservoir operation (Gangrade et al., 2018) may introduce further uncertainties to the PMF estimate and consequently the resulting surface inundation area. The 2017 Hurricane Harvey precipitation near Houston, Texas, is reported to exceed the Hydro-meteorological Report No. 51 (HMR51; Schreiner and Riedel, 1978) 72-h PMP estimates at 5000 mi² and 10,000 mi² scales (Kao et al., 2019), suggesting that an extremely large PMP-scale storm is physically possible. Considering that there has not been a focused federal effort since the publication of HMRs, it is of critical importance to advance our concept and practice from the conventional, deterministic treatment of PMP/PMF to an ensemble-based, probabilistic flood mapping approach to better analyze and quantify the vulnerability of critical energy-water infrastructures in a changing environment.

In this study, building upon our prior work involving PMP/PMF simulations (Rastogi et al., 2017; Gangrade et al., 2018), we present a

high-resolution, process-based, hydro-meteorological modeling framework to produce probabilistic flood inundation maps for PMF. The main objectives of the study are (1) to employ an ensemble-based approach to translate uncertainties associated with PMP to flood inundation maps, (2) to prepare probabilistic flood inundation maps illustrating uncertainties with the flood hazard modeling chain of PMF, and (3) to quantify the potential impacts of environmental change on the inundation areas of PMF. The study area includes areas immediately upstream and downstream of the Allatoona Dam in Georgia, US. For PMP, we used Weather Research Forecasting (WRF), a numerical weather simulation model (Skamarock et al., 2008) to create an ensemble of 120 storms. The input forcings to the WRF model is provided by reanalysis as well as climate projections as detailed in Rastogi et al. (2017). These 120 PMP storms were then used to conduct PMF estimates using the Distributed Hydrologic Soil Vegetation Model (DHSVM; Wigmosta et al., 1994) as described by Gangrade et al. (2018). The ensemble of PMF hydrographs was further used to drive a high-resolution, graphics processing unit– (GPU) accelerated 2-dimensional (2D) dynamic wave flood model (Flood2D-GPU; Kalyanapu et al., 2011) to simulate the spatiotemporal evolution of PMF and to develop ensemble-based PFMs. Apart from better quantifying uncertainties, compared with the deterministic approach, the ensemble-based flood mapping approach allowed us to better visualize the potential impacts of PMF through a spatially explicit, more intuitive manner. This study is the first of its kind that implements a high-resolution modeling framework to assess changes in flood regime through an ensemble-based approach for PMF to account for a changing climate and other factors. The study also includes a relative sensitivity experiment to evaluate the sensitivity of various factors in the modeling chain, including inputs such as precipitation, hydrologic model antecedent conditions, and hydraulic model parameters. Although the proposed study is presented for a selected watershed, the methodology can also be adopted for other locations with similar climates and geographical settings for broader applications.

This study is organized as follows: Section 2 provides an overview of the study area, methodology, and data; Section 3 presents results and associated discussion; and Section 4 summarizes and concludes the study.

2. Methods

2.1. Study area

This study focuses on the Etowah Watershed located in the north-western Georgia, US. We selected this watershed because it includes a major reservoir and urban areas and lies in a relatively flat topographic region, allowing transposition of PMP storms. The Etowah Watershed has an estimated drainage area of 4821 km² (1861 mi²; Fig. 1) and is a part of the Alabama-Coosa-Tallapoosa (ACT) River Basin. It drains parts of 15 counties in Georgia and covers major urban areas including the city of Cartersville and parts of Atlanta's metropolitan area such as Woodstock, Marietta, and Alpharetta. The Etowah Watershed includes a large multi-purpose reservoir, Allatoona Lake and Dam, owned and operated by the US Army Corps of Engineers (USACE), with a maximum storage capacity of roughly 826.5 million m³ (the second-largest dam in the ACT River Basin). While the headwaters of Etowah Watershed include mountainous areas (such as the Piedmont mountains), the topography of the rest of the watershed is moderate, with elevations ranging from 176 m (577 ft) to 1147 m (3763 ft) as per the National Elevation Dataset (NED; Gesch et al., 2002). The region receives roughly 1336 mm of annual precipitation, predominantly in the form of rainfall, with light snowfall in the headwater region. The major soil types include silty loam and sandy loam. According to the National Land Cover Database 2006 (Fry et al., 2011), 61% of the basin is covered by forests, 18.5% lies under small vegetation, and 18.5% falls in the developed category.

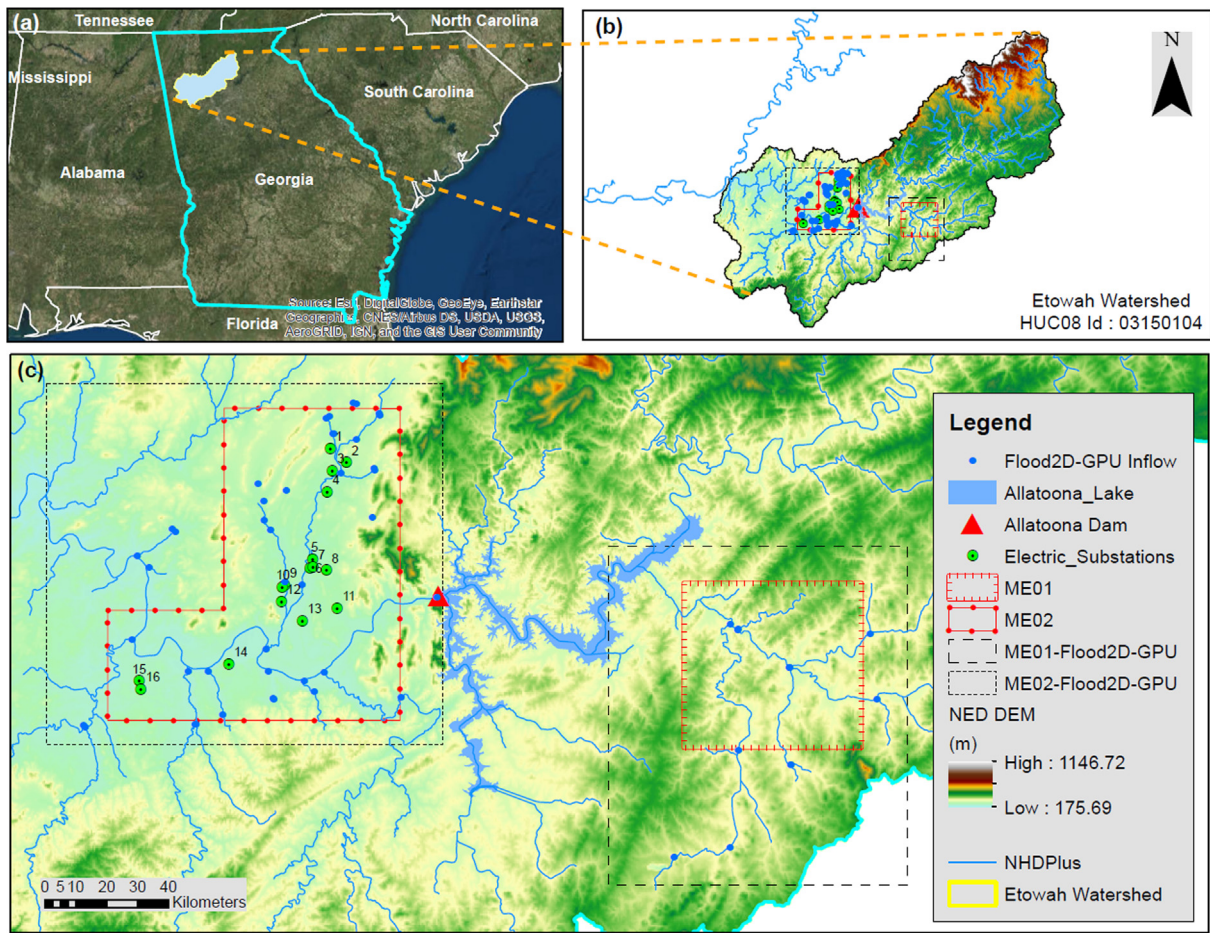


Fig. 1. Etowah Watershed with two selected areas of interest, ME01 and ME02, along with Flood2D-GPU setup including computational domains, DEM, inflow locations, and stream network. The inserted panel at left shows the overall location of Etowah Watershed in Georgia, US.

The main critical infrastructure located in the Etowah Watershed is the Allatoona Dam which produces hydroelectric power for the region. The PMFs developed through the WRF and DHSVM cover both the upstream and downstream areas of the Allatoona Lake and Dam. To further demonstrate the applicability of probabilistic flood maps for other energy infrastructures, we also evaluate 16 selected electrical substations (obtained from Homeland Infrastructure Foundation-Level Data; Fig. 1) in the watershed. Four different types of modeling/analysis domains were used in this study. The WRF meteorological and DHSVM hydrologic modeling domains covered the Etowah Watershed as well as the entire ACT River Basin (see Rastogi et al., 2017, and Gangrade et al., 2018, for domain details). Two Flood2D-GPU modeling domains (i.e., 358 km² ME01-Flood2D-GPU and 507 km² ME02-Flood2D-GPU in Fig. 1) were set up within the Etowah Watershed, and final analysis was performed for two slightly smaller analysis domains (ME01 and ME02). The two regions, upstream (ME01) and immediately downstream (ME02) from Allatoona Dam, were selected such that they cover parts of the Atlanta metropolitan region and the City of Cartersville in the Etowah Watershed. The computational domains of

Flood2D-GPU were set to be larger than the analysis domains to avoid potential backwater effects and computational domain boundary artifacts.

2.2. Simulation setup

We used a process-based, high-resolution modeling framework to develop multi-ensemble flood inundation maps associated with PMF estimates. The main steps involved (1) simulation of PMP storms, (2) simulation of PMF hydrographs, and (3) simulation of flood regimes. A brief overview of the methods follows.

2.2.1. Simulation of PMP

The simulation of PMP storms was performed using a mesoscale numerical weather model, WRF version 3.6. The WRF model is driven using boundary forcings from: a) a reanalysis dataset: Climate Forecast System Reanalysis I (CFSR; Saha et al., 2010), and b) a global climate model: Community Climate System Model version 4 (CCSM4; Gent et al., 2011). The WRF model, setup at a 9 km and 3 km (double nested)

Table 1
List of 120 events used to generate moisture-maximized storms under historic and future climate forcings.

Storm Set	No of storms	Time Period	Forcings Source
CFSR-CT	30	1981–2011	CFSR Reanalysis (Control Simulation)
CCSM4-BL	30	1981–2005 (historical) 2006–2010 (RCP 8.5)	CCSM4 (Baseline Simulation)
CCSM4-F1	30	2021–2050 (RCP 8.5)	CCSM4 (Near Future Simulation)
CCSM4-F2	30	2071–2100 (RCP 8.5)	CCSM4 (Far Future Simulation)

horizontal grid resolutions, was driven for 120 selected storms (Table 1) using the relative humidity maximization (RHM) method to simulate PMP. Before PMP estimation, WRF parameterization was selected by testing the simulated 3-day rainfall depth against the PRISM (Daly et al., 2008) and Daymet (Thornton et al., 1997) precipitation datasets to assess and compare WRF performance. PMP was then estimated using the selected parameterization with the RHM method, which maximizes the relative humidity of the entire atmospheric column to 100 % at initial and boundary conditions following Ohara et al. (2011) and Ishida et al. (2015). The PMP outputs were stored at 1-hourly temporal resolution. The readers are referred to Rastogi et al. (2017) for further technical details regarding PMP estimation and WRF performance evaluation.

In addition, Hydrometeorological Report (HMR) 51 (Schreiner and Riedel, 1978) and HMR52 (USACE, 1984) were used to obtain conventional PMP rainfall estimates for the study area. This enables a comparison of ensemble-based simulations with the conventional deterministic approach and serves as a reference. The ensemble approach relies on identifying the most critical PMF event based on hydrologic and hydraulic simulations for each of the PMP storms, as opposed to one deterministic event under conventional approach estimated using synthetic hyetographs. The ensemble-based approach leads to better understanding of the uncertainty associated with PMP estimates.

2.2.2. Simulation of PMF

The PMF simulations were conducted by using each of the 120 moisture maximized storms as the meteorological forcing input to drive a high-resolution DHSVM. DHSVM was selected because of its wide applications in hydroclimate impact assessments and its capability to generate high-resolution streamflow data required to drive the consequent hydrodynamic flood models. DHSVM is a distributed, process-based model and performs water/energy balance calculations to account for various hydrological processes. The model uses precipitation, air temperature, radiation (both longwave and shortwave), wind speed and relative humidity as input datasets (Wigmosta et al., 1994 and 2002; Storck et al., 1998). The DHSVM setup for the Etowah Watershed was obtained from Gangrade et al. (2018), which is a part of a larger modeling effort performed for the ACT River Basin. The DHSVM simulation was performed at the 3-hourly time step and 90-m horizontal grid resolution from 1980–2012. The 90-m NED is used as the base digital elevation model (DEM) map for DHSVM simulation. Further, the soil (Miller and White, 1998) and land-use and land-cover data (NLCD; Fry et al., 2011) were resampled at the base map resolution to serve as inputs to hydrologic simulation. The stream network was obtained from the National Hydrography Dataset Plus (McKay et al., 2012). Readers are referred to Gangrade et al. (2018) for associated detailed technical descriptions regarding setup, calibration and validation.

To simulate PMF specifically for the Etowah Watershed, for every storm listed in Table 1 (Section 2.2.1), the largest 72-h average precipitation (which is the largest duration commonly used by HMR reports to estimate PMP) over the watershed was identified from the WRF output and transpositioned to the center of the Etowah Watershed as an input for DHSVM. Given the relatively smooth topography in the ACT River Basin (compared with other mountainous regions in the US), storms within the basin can be considered meteorologically transpositionable. This enables identification of the most critical PMP input for the study area and ensures that the PMP storm is captured by the watershed. The simulated precipitation depth from the most inner WRF domain (as explained in Section 2.2.1) was further re-gridded/aggregated as 3-hourly inputs to DHSVM at a 4-km horizontal grid resolution radar rainfall format. Following the Nuclear Regulatory Commission guidelines, a critical meteorological sequence was used for PMF estimation (Prasad et al., 2011). The meteorological sequence included 40% of 72-hr PMP (antecedent precipitation), followed by no precipitation for 72 hours, and then a full (100%) 72-hr PMP (critical precipitation). Fully saturated moisture conditions were used at the

beginning of the DHSVM simulations. This approach provides an ensemble of simulated DHSVM streamflow hydrographs for each set of storms sets as specified in Table 1 (i.e., CFSR-CT, CCSM4-BL, CCSM4-F1, and CCSM4-F2).

The ensemble PMF hydrographs obtained above were also compared against conventional PMF driven by conventional PMP rainfall estimates calculated for Etowah Watershed using HMR51 and HMR52. The detailed methodology is described in Gangrade et al. (2018).

2.2.3. Simulation of flood regime

The hydrodynamic flood simulation was performed using the computationally enhanced version of the 2D hydraulic model Flood2D-GPU (Marshall et al., 2018), originally developed by Kalyanapu et al. (2011). Flood2D-GPU uses a first-order accurate upwind finite difference scheme in solving the nonlinear hyperbolic shallow water Saint Venant equations, which are a simplified version of the Navier-Stokes equations with horizontal momentum and continuity equations integrated over water depth. The model implements on a structured grid to take advantage of the uniform grid structure of the DEM data. The computational performance of the Flood2D-GPU model was improved using a hybrid Message Passing Interface (MPI) and Compute Unified Device Architecture (CUDA). The model speed-up for the MPI + multiple GPU version was up to $18\times$ compared with an identical single-process Open Multi-Processing (OpenMP) version (Marshall et al., 2018). Benefitting from GPU acceleration, the high performance of Flood2D-GPU allowed us to perform ensemble simulation for two domains: ME01 ($\sim 400,000$ grid cells, 360 km^2) and ME02 ($\sim 563,000$ grid cells, 507 km^2). The simulations were conducted on the Titan supercomputer maintained by the Oak Ridge Leadership Computing Facility and used ~ 1 million computing hours for ensemble flood simulation.

The key input data required for Flood2D-GPU include DEM, surface roughness (Manning's n value), inflow source locations, and the corresponding streamflow hydrographs. In this study, both 30-m and 10-m resolution DEM data were obtained from NED. We tested several commonly used Manning's n values and selected 0.035 as the default value (discussed in Section 3). For the selection of inflow locations (Fig. 1), we first identified the main upstream NHDPlus channel segments that flow into the Flood2D-GPU simulation domain. We then selected a series of additional NHDPlus segments (with approximately 50 km^2 incremental drainage areas) to input the incremental streamflow hydrographs. The corresponding hydrographs for each of the 120 storms were extracted using high-resolution hydrologic outputs from DHSVM at 3-h time-steps for both domains (i.e., ME01 and ME02). The Flood2D-GPU was driven by 5-day hydrographs that capture the peak discharge of each storm event, and the output was stored at a 10 minute temporal resolution for each storm. The Flood2D-GPU performance is evaluated and presented in the Results and Discussion section. The current model setup captures riverine or fluvial floods; the pluvial flood simulation, an important aspect for flood map generation to support decision making, shall be incorporated in the future model improvements.

Apart from the default simulations driven by simulated PMF hydrographs, an additional set of 120 flood simulations were conducted for ME02 (downstream of Allatoona Dam) with modified upstream inflow to understand the maximum flood retention capacity under idealized reservoir operation (denoted as ME02R). At the stream segment immediately downstream of the Allatoona Lake and Dam, the volume equal to the maximum storage capacity of the Allatoona reservoir (i.e., 826.5 million m^3) was subtracted from the peak of the PMF hydrograph. In other words, this ME02R simulation assumes that the reservoir can be fully emptied right before a PMF event, remains structurally intact throughout the entire event, and is operated optimally to reduce the peak discharge of a PMF event. The modified hydrograph in addition to natural flow from other tributaries served as an input for ME02 to drive Flood2D-GPU for each of the 30 storm sets from CFSR-CT, CCSM4-BL, CCSM4-F1, and CCSM4-F2. This hypothetical discharge

scenario is mainly used to identify the maximum possible downstream flood inundation area reduction under the most optimistic flood management operation. Given that the actual reservoir operation is unlikely to beat this optimal scenario, the actual PMF inundation area under the protection of a reservoir should be within the range between ME02 and ME02R.

2.3. Probabilistic flood map

For each simulated PMF flood event (realization), the Flood2D-GPU simulation outputs were stored at a 10-minute temporal resolution for the duration of the flood. These outputs were first post-processed to obtain the maximum flood inundation extents arising from the event. A minimum threshold of 10 cm flood depth was used to differentiate a cell as flooded vs. not flooded (Kalyanapu, 2011) during the post-processing step. Using the maximum flood inundation extents for every flood event as an input, the probabilistic value of flooding for any given cell was then calculated using Eq. (1) (Kalyanapu et al., 2012). Given that these moisture maximized storms were selected by the 30 largest storms within a 30-year period (Rastogi et al., 2017), each storm is weighed equally in this study. This approach was used to produce one PFM for each of the storm sets (i.e. CFSR-CT, CCSM4-BL, CCSM4-F1, and CCSM4-F2) for both ME01 and ME02.

$$P_{cell} = \frac{\sum_{i=1}^{i=N} X_i}{N} \quad (1)$$

where

P_{cell} = probability to flood for any given cell
 X_i = 0 (dry) or 1 (wet) for realization 'i'
 N = total number of realizations/flood event simulations.

The PFM presents a spatial map of conditional probability of flooding given a moisture-maximized extreme storm event has occurred at the region of interest. The PFMs were generated for the two model domains ME01 and ME02 for each of the 30 storm sets for CFSR-CT, CCSM4-BL, CCSM4-F1, and CCSM4-F2. The flood simulations are referenced by adding the subscript ME01, ME02, and ME02R after the name of the storm set. For example, CFSR-CT-ME01, CFSR-CT-ME02, and CFSR-CT-ME02R refer to PFMs generated for CFSR-CT storms for model domains ME01 and ME02 under natural flow and ME02 under reservoir regulation, respectively.

3. Results and discussion

3.1. Flood2D-GPU performance

The performance of Flood2D-GPU was evaluated by comparing the simulated 100-year flood inundation extents against a benchmark data set from FEMA (100-year flood zones or Zone A/AE; Wing et al., 2017; Alfieri et al., 2014) for ME01. The first step in the process involved the estimation of a 100-year peak streamflow (Q_{100}) through standard frequency analysis at the outlet of ME01 using guidelines from Bulletin 17B prepared by the Interagency Advisory Committee on Water Data (1982). The continuous streamflow data from the control simulation (i.e., DHSVM driven using observed historic precipitation from Daymet) for a period of 32 years (1981–2012) served as inputs for frequency analysis. The annual maximum series (AMS) of peak discharge ($Q_{max,year}$) was extracted from the hydrograph at the outlet of ME01. A log-Pearson Type III distribution was then fitted to the AMS using a skewness parameter obtained for the region based on Plate 1 of Bulletin 17B. The results from the flood frequency analysis are illustrated in Fig. 2. Based on the annual maximum peak discharges for a period of 32 years, we obtain a Q_{100} value of 18,956 ft³/s at the outlet of ME01.

In the next step, we employed an ensemble-based approach to

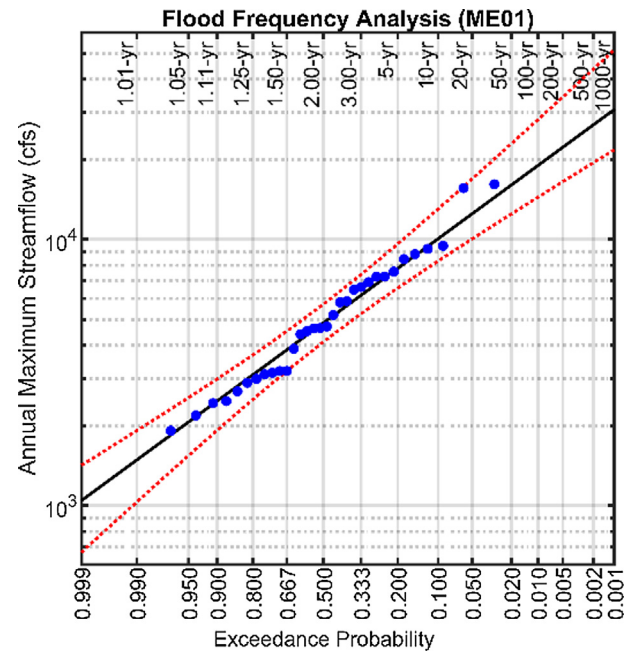


Fig. 2. Standard flood frequency analysis for ME01 according to the guidelines of Bulletin 17B.

validate Flood2D-GPU, as a single storm might not be able to capture the spatial variability across the watershed and might result in under-estimation of flood extents. For each annual maximum peak discharge event, the hydrographs at each inflow location (Fig. 1) were abstracted (i.e., 32 events from 1981 through 2012). These hydrographs were then re-scaled to match the estimated 100-year peak discharge value and served as inputs to Flood2D-GPU to conduct the simulation at 30-m spatial resolution. The rescaling of the hydrographs was performed by multiplying the hydrographs by a rescaling factor (R_{yr}) calculated at each year as $R_{yr} = Q_{100}/Q_{max,yr}$, so that the peak streamflow at the domain outlet of each simulation is controlled at the same Q_{100} value. This approach retains the relative streamflow magnitude across all tributaries, and allows us exploring the spatial variability and uncertainty across the ensemble members. The ensemble simulation resulted in 32 flood inundation maps. The maximum inundation area was then identified from the 32 maps and compared against a FEMA 100-year flood map rasterized to the same 30-m resolution. The flood maps were compared based on a binary (flooded = 1, not flooded = 0) classification scheme, as presented in Table 2. The comparison was performed for the analysis domain ME01; and the smaller stream segments that had no inflow locations (because of modeling constraints/limitations) were excluded. The vector-based FEMA flood extents for the region of interest were rasterized to the Flood2D-GPU grid to enable a direct comparison.

Fig. 3 presents a comparison of 100-year flood inundation extents obtained from Flood2D-GPU and FEMA. A visual inspection reveals that the 100-year flood zones simulated by Flood2D-GPU are largely consistent with the FEMA flood zones. While there may also be inaccuracies and uncertainties associated with FEMA flood zones, this study uses the FEMA data as a benchmark to evaluate the overall reasonableness of

Table 2

Contingency table for the analysis domain in ME01 represented as a fraction of total number of cells in the analysis domain.

Cells	Wet in Model (M1)	Dry in Model (M0)
Wet in FEMA (B1)	0.0804 (M1B1)	0.0175 (M0B1)
Dry in FEMA (B0)	0.0162 (M1B0)	0.8859 (M0B0)

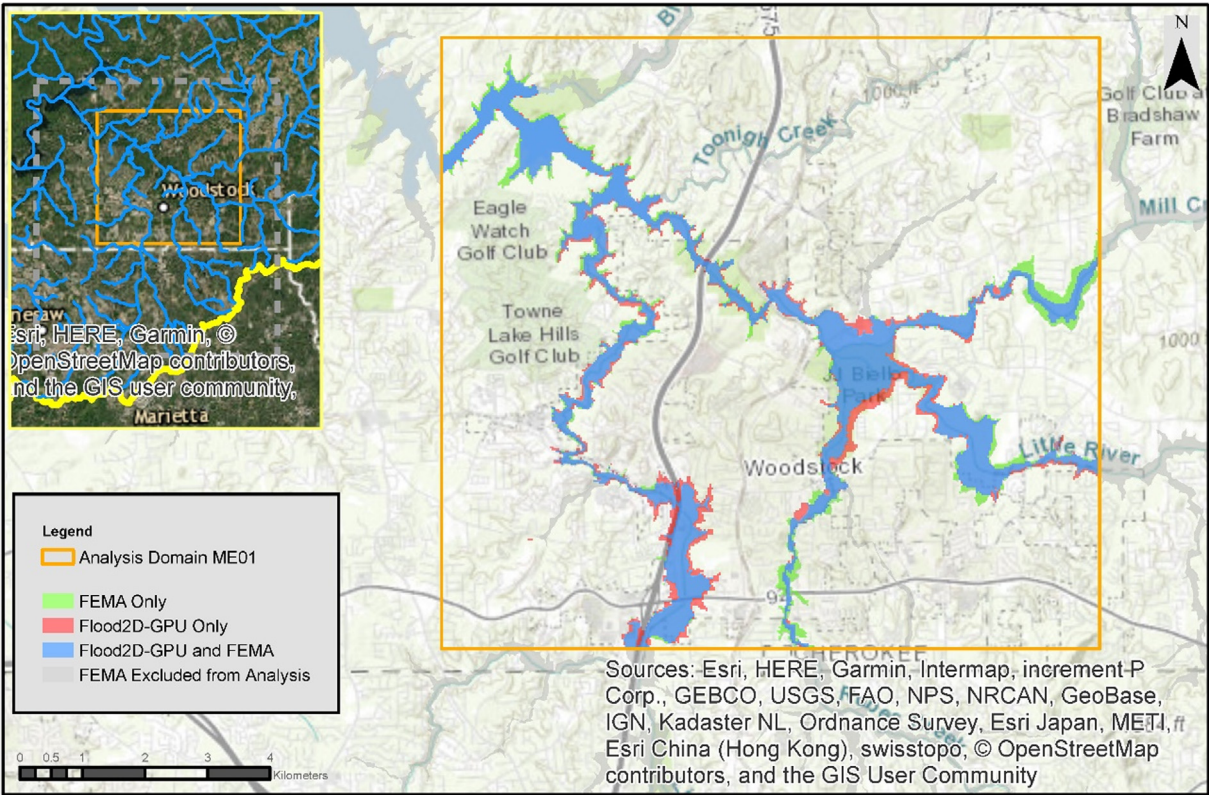


Fig. 3. A comparison of flood inundation spatial extents obtained from Flood2D-GPU and FEMA for 100-year flood events. The regions flooded with both Flood2D-GPU and FEMA flood zones are presented in blue. The regions in red/green represent the cells flooded only by Flood2D-GPU/FEMA. The FEMA zones excluded from this evaluation because of model or other data limitations are presented in gray.

Flood2D-GPU.

Four key metrics including critical success (C), hit rate (H), false alarm (F), and error (E) were estimated to quantify Flood2D-GPU performance (Table 3). H provides a measure of the model to accurately predict benchmark flood extents; however, it does not penalize for overprediction. Flood2D-GPU obtained $H = 0.82$ for ME01, revealing the model can accurately predict 82% of the FEMA flood zones. F, which measures overprediction, is estimated as 0.17, demonstrating that 17% of the grid cells were falsely reported as flooded by the model. The C equivalent to the F-squared statistics, a common metric to evaluate spatial extents for flood studies (Bates and De Roo, 2000), is estimated as 0.70, providing an overall measure of fit. The C metric adds a penalty to H for any overprediction and underprediction. In addition, the fact that E for Flood2D-GPU is less than 1 (0.93) suggests an overall tendency of the model to underpredict, predominantly in the upstream reaches close to inflow boundary conditions.

These key metrics suggest that Flood2D-GPU performance is on a par with the acceptable range of these metrics provided in the literature (Alfieri et al., 2014; Wing et al., 2017). For instance, Alfieri et al. (2014) obtained H values between 0.59 and 0.78, and C values between 0.43 and 0.65 for a flood simulation at 100-m resolution across selected areas in Germany and the United Kingdom compared with national/regional hazard maps. Wing et al. (2017) performed a similar

evaluation for validation of a flood hazard model for the conterminous US using FEMA flood zones as a benchmark, with H values as 0.685 and 0.815 and C values of 0.55 and 0.50 for 90 m and 30 m spatial resolutions, respectively. The results indicate overall satisfactory performance of the Flood2D-GPU in comparing spatial extents for 1 in 100-year event against the equivalent flood inundation zone obtained from FEMA.

3.2. Ensemble PMF hydrographs and comparison with deterministic approach

This section presents the ensemble PMF hydrographs for each of the four sets of moisture-maximized storms (i.e., CFSR-CT, CCSM4-BL, CCSM4-F1, and CCSM4-F2) at the outlet of the Etowah Watershed (Fig. 4). The hydrographs with the largest peak discharge are presented in thick lines in Fig. 4 and are individually presented in Fig. 5a. For further comparison, the PMF hydrograph from the conventional approach (HMR based) is also presented for the Etowah Watershed (Fig. 5a). The range of peak discharge values for these events is presented in Fig. 5b for Etowah Watershed and at the outlets of computational Flood2D-domains ME01 and ME02 in Fig. 5c and d, respectively.

The results indicate that peak discharges obtained for CCSM4-BL

Table 3
Key flood model performance metrics calculated for ME01 for a 100-year ensemble flood event. Adopted from Wing et al. (2017).

Criterion	Formula	Calculated Value	Range	Description
Hit rate (H)	$M1B1/(M1B1 + M0B1)$	0.82	0 – 1	Measure of tendency of model to accurately predict the benchmark flood extents
False alarm ratio (F)	$M1B0/(M1B0 + M1B1)$	0.17	0 – 1	Measure of tendency to overpredict flood extent
Critical success index (C)	$M1B1/(M1B1 + M0B1 + M1B0)$	0.70	0 – 1	Measure of fit with penalty for overprediction and underprediction
Error (E)	$M1B0/M0B1$	0.93	0 – infinity	Measure of tendency toward overprediction or underprediction

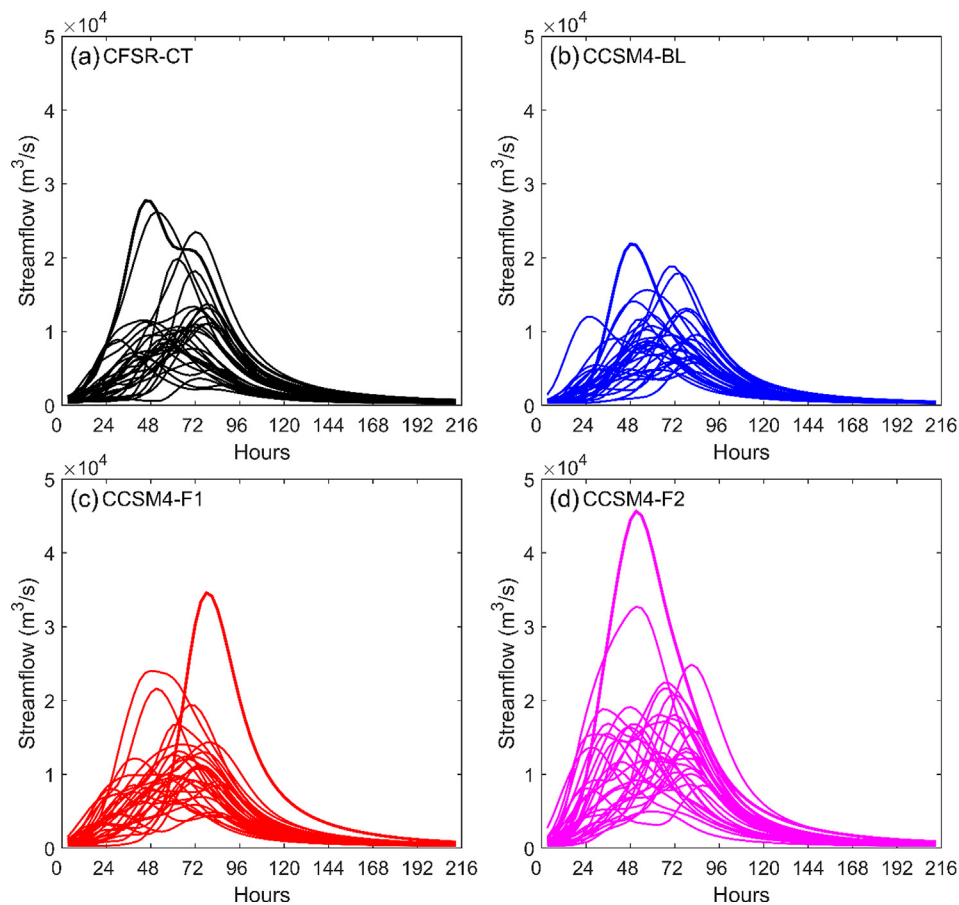


Fig. 4. Ensemble PMF hydrographs for each set of the moisture-maximized storms (listed in Table 1) at the outlet of Etowah Watershed. The hydrograph yielding the highest peak discharge in each set of storms is highlighted with a thick line.

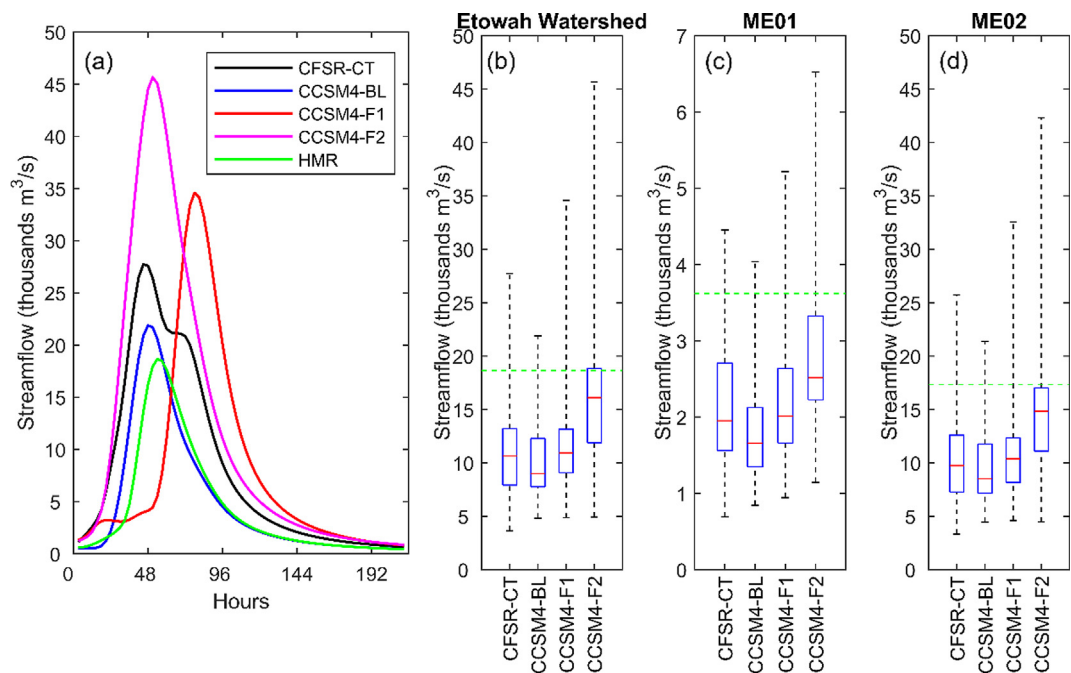


Fig. 5. PMF hydrographs selected based on peak discharge for Etowah Watershed (Panel a) and range of peak discharge for each set of simulations (CFSR-CT, CCSM4-BL, CCSM4-F1, and CCSM4-F2), with corresponding HMR scenario values marked as a green dashed line, for Etowah Watershed and ME01 and ME02 (Panels b, c and d respectively).

Table 4

Key ensemble PMF peak discharge statistics for domains ME01, ME02, and at the outlet of the Etowah Watershed.

Scenario	Etowah Watershed				ME01				ME02			
	Min (m ³ /s)	Mean (m ³ /s)	Median (m ³ /s)	Max (m ³ /s)	Min (m ³ /s)	Mean (m ³ /s)	Median (m ³ /s)	Max (m ³ /s)	Min (m ³ /s)	Mean (m ³ /s)	Median (m ³ /s)	Max (m ³ /s)
CFSR-CT	3628	11,883	10,645	27,732	692	2,255	1,951	4,453	3,326	11,061	9,761	25,726
CCSM4-BL	4815	10,255	8996	21,874	843	1850	1657	4038	4459	9594	8507	21,379
CCSM4-F1	4874	12,184	10,923	34,591	943	2246	2013	5219	4592	11,319	10,382	32,555
CCSM4-F2	4925	16,704	16,098	45,660	1144	2800	2517	6523	4485	15,517	14,824	42,312
HMR			18,654				3618				17,322	

and HMR are comparable in magnitude with maximum peak discharge values of 21,874 m³/s and 18,654 m³/s, respectively. Although the deterministic HMR peak discharge is less than the maximum event in each set of the hydrographs, it is larger than more than 75% of the ensemble members and lies among the top quartile of all events. In addition, the HMR based deterministic peak discharge is 82% larger than the ensemble mean peak discharge of all CCSM4-BL members (Table 4), suggesting the relative magnitude of the deterministic HMR approach.

The maximum peak discharge for CFSR-CT (27,732 m³/s) is greater than for CCSM4-BL. This higher discharge could be attributed to higher PMP estimates for CFSR-CT, demonstrating the effect of the choice of meteorological forcings on PMF (Gangrade et al., 2018). The effects of climate change on maximum peak discharge indicate a significant increase in peak discharge magnitude, with an increase of approximately 58% for the near future time period (CCSM4-F1; 2021–2050) and 109% for the far-future period (CCSM4-F2; 2071–2100). The comparison is performed with reference to the peak discharge magnitude obtained for the baseline period CCSM4-BL. These changes could be attributed to increased PMP estimates projected in the future periods resulting from the intensification of the hydrologic cycle caused by atmospheric warming. Readers are referred to Rastogi et al. (2017) and Gangrade et al. (2018) for further technical details.

The results demonstrate a large variability in the hydrograph shapes and peak discharge values (Figs. 4, 5b–d). In addition to the key factor (e.g., PMP magnitude), the variability in the hydrographs can be attributed to spatiotemporal rainfall structure and watershed heterogeneity. The results also highlight the range of uncertainties captured in terms of streamflow estimates, which are often missing in the conventional, deterministic estimation of PMF. Here we mainly focus on the range of streamflow variability that corresponds to a set of moisture-maximized storms. Similar concepts can also be followed to develop ensemble hydrographs that address other possible sources of uncertainties (e.g., timing, parameterization).

3.3. Development of probabilistic flood maps

An ensemble-based approach involves analyzing a collection of simulated flood events corresponding to multiple hydrographs and peak discharge magnitudes. Generally, the most extreme or worst-case scenario is selected by choosing the single PMF hydrograph with the maximum peak discharge. In this section, we analyze the effects of ensemble PMF in terms of flood inundation area by translating these hydrographs into probabilistic flood inundation maps and comparing the results with flood extents obtained via the conventional deterministic approach. This comparison is intended to illustrate flood damages/extents resulting from PMF events and associated uncertainties.

The PFMs are presented for each of the 30 moisture-maximized storms (Fig. 6, Panels a through d for ME01, Panels e through h for ME02, and panels i through l for ME02R). The results are presented in term of conditional probability of flooding for a given cell, assuming a moisture-maximized storm has occurred in the region. Panels a and e also include the deterministic flood extents obtained from Flood2D-

GPU driven by conventional HMR PMF, presented as white contours overlaid on top of the probabilistic flood maps. In addition, the range of maximum flood inundation area associated with each storm event is presented in Fig. 7 for ME01 (Panel a), ME02 under natural flow condition (Panel b), and ME02R under ideal reservoir regulation (Panel c).

A comparison of the maximum flood inundation extent for the domain upstream of Allatoona Lake and Dam (ME01; Fig. 6a), obtained by the conventional (HMR-based) approach (15.56 km²), is very similar to the maximum flooding extent of CFSR-CT-ME01 (16.83 km²) and CCSM4-BL-ME01 (16.32 km²), resulting in 8.2 % and 4.9% respective increments in inundation area compared with HMR. On the other hand, the downstream domain (ME02; Fig. 6e) has a larger difference in flood extent obtained from the HMR approach (96.6 km²) compared with the maximum flood extents of CFSR-CT-ME02 (117.9 km²) and CCSM4-BL-ME02 (101.5 km²); the results are 22.1 % and 5.1% respective increments in inundation area compared with HMR. A comparison of panels 6e and 6i in Fig. 6 reveals the maximum possible flood reduction by the Allatoona reservoir due to its regulation of PMF-scale events in the immediate downstream areas. Ideal reservoir operation results in a decrease in the maximum flood inundation area of 9.5% in the CFSR-CT case.

Given the projected future climate conditions, the simulated maximum inundation area reveals a likely increase in both near future (CCSM4-F1) and far future (CCSM4-F2) periods. For ME01, the projected maximum inundation areas are 17.6 km² for CCSM4-F1 and 19.1 km² for CCSM4-F2, which suggest 8% and 17% increases when compared with the 16.3 km² CCSM4-BL-ME01 baseline value (Fig. 7a). Similarly, a total of 121.2 km² (108.7 km²) and 135.7 km² (128.4 km²) in the maximum inundation area is projected for ME02 (ME02R) for CCSM4-F1 and CCSM4-F2, and they suggest 19% (22%) and 34% (44%) increases when compared with the 101.5 km² (88.9 km²) CCSM4-BL-ME02 (CCSM4-BL-ME02R) baseline value. The results indicate that the percentage increase in maximum inundation area is projected to be higher for ME02R than for ME02, mainly due to a smaller ME02R baseline value.

Given the wide range of areal extents produced for each set of moisture-maximized storms, further insight into flood characteristics (e.g., flood inundation area, gauge height) using hydrologic/meteorological parameters can improve the understanding of flood zones. The relationship between peak discharge and maximum flood inundation area is presented in Fig. 8. Although the maximum flood inundation area is highly correlated to the peak discharge at the outlet of each model, the relationship is nonlinear, with a higher variance observed for ME02 (Fig. 8b) than for ME01 (Fig. 8a). This finding was mainly attributed to the relatively flat topography in ME02. The variability demonstrates that a similar peak discharge could result in varying extents of flood inundation which could be attributed to hydrograph characteristics (including timing, sequence, and total flood volume) and spatial variations in streamflow. For instance, two storms with maximum peak discharges of 11,112 m³/s and 11,504 m³/s, respectively, can produce maximum flood inundation areas of 102.1 km² and 81.32 km² for ME02 (Fig. 8b).

The results suggest that a single peak discharge value for PMF

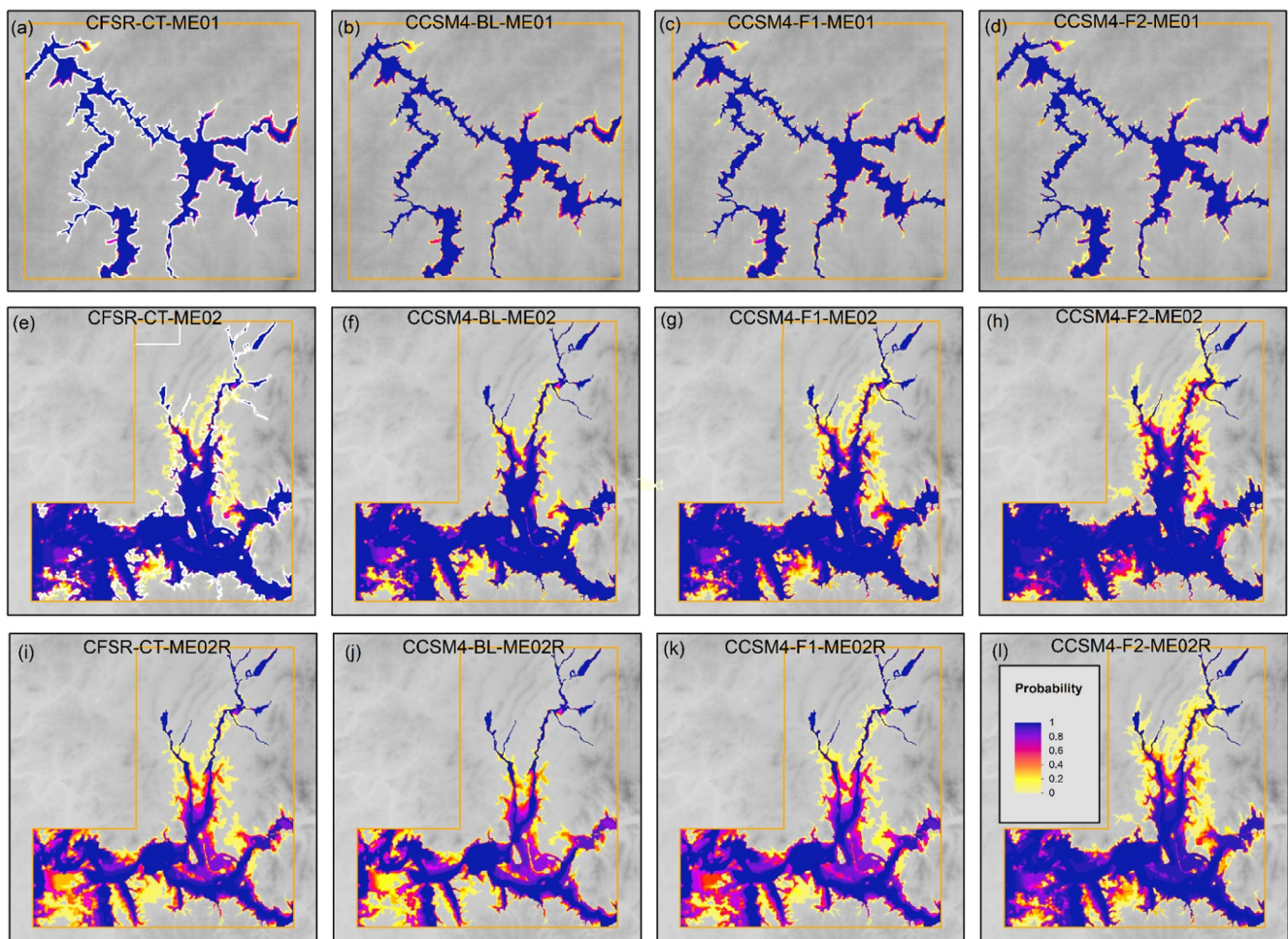


Fig. 6. Ensemble flood maps for domain upstream of Allatoona Lake ME01 (a through d), and domain ME02 downstream of Allatoona Lake (e through h), and ME02 with reservoir regulation (i through m) for each of the storm sets CFSR-CT, CCSM4-BL, CCSM4-F1, and CCSM4-F2. Panels a and e also show HMR52-based flood extents in white contour.

obtained using the conventional approach cannot capture such variations in flood impacts. The results further highlight the value of an ensemble-based approach compared with current deterministic methods for more comprehensive understanding of flood damage resulting from an extreme event.

3.4. Potential changes in flood impacts arising from PMF

In this section, we use the PFM to examine the potential changes in the flood regime and its impacts on infrastructure/urban developments under projected future climate conditions. To illustrate how the conditional probability of flooding due to moisture maximized storms changes in different periods, the difference in probability of flooding at each grid among CCSM4-BL, CCSM4-F1, and CCSM4-F2 for each domain ME01, ME02 and ME02R was calculated and is summarized in Fig. 9. The grid cells that are consistently flooded (i.e., probability = 1) or non-flooded (i.e., probability = 0) in all inundation maps across all storms (CCSM4-BL, CCSM4-F1, and CCSM4-F2) were excluded from the analysis.

The results indicate that the overall probability of flooding will increase by up to 30% in CCSM4-F1 across ME01, ME02, and ME02R, where most grid cells show increasing probability ranging between 0 and 0.15. Similarly, the histogram for CCSM4-F2 indicates that the overall probability of flooding will increase by up to 60% for CCSM4-F2 for each domain ME01, ME02, and ME02R, with most cells showing positive increases ranging between 0 and 0.25. This process allows the

identification of other areas that may be more susceptible to PMF-scale flooding in addition to the most vulnerable areas (i.e., probability = 1).

To demonstrate the potential application of this framework, the analysis was further expanded to demonstrate the utility of PFMs as a tool to identify potential hazards to electricity grid infrastructure arising from PMF events. The vulnerability of 16 selected electric substations (from the Homeland Infrastructure Foundation-Level Data; Fig. 1) for ME02 was evaluated and additional ensemble information, such as duration of flooding and median flood depths, is presented in Fig. 10.

These results identify the substations at risk of flooding given a PMF event has occurred. Of 16 substations, 8 substations (#6, 7, 9, 10, 12, 13, 14, and 15) demonstrated a high probability of flooding (> 0.75) for ME02 under unregulated flow condition for CCSM4-BL. The mean duration of flooding and median flood depths is likely to show an increase in CCSM4-F1 and CCSM4-F2 compared with CCSM4-BL. Similarly, the substations currently not at risk of flooding in CCSM4-BL (for instance, #1, 2, 3, 5, and 8) have a higher chance of flooding in future time periods, i.e. CCSM4-F1 and CCSM4-F2. Further, additional information from the ensemble approach—such as distribution of duration of flooding and median floods depths—has the potential to reduce the likelihood of Type I and Type II decision errors in risk management. Such risk identification research can help improve current flood mitigation features while also equipping decision makers with information that can be used in strategic planning and development of future urban areas and/or critical infrastructure.

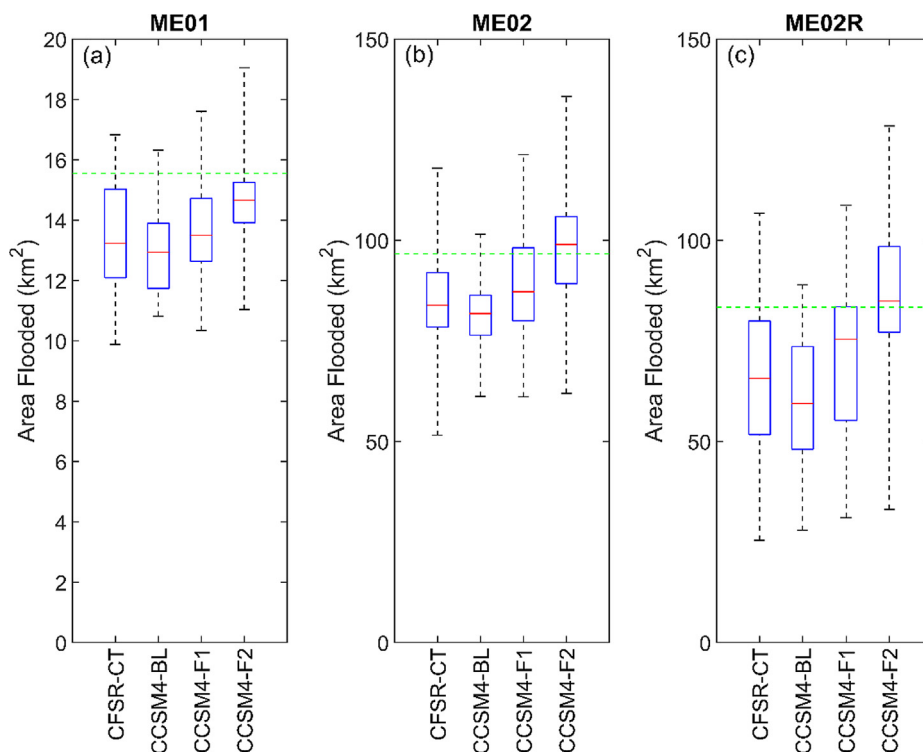


Fig. 7. Boxplot showing the range of area under inundation for each of the storm sets for domain upstream of Allatoona Lake ME01 (Panel a), and domain ME02 downstream of Allatoona Lake under natural flow condition (Panel b), and ME02 under reservoir regulation (Panel c). The area inundated under HMR scenario is marked with a green dashed line in each of the panels.

3.5. Sensitivity analysis

To understand the overall and relative sensitivity of flood inundation to various factors—such as meteorological forcings, climate change, hydraulic and hydrologic model inputs, and parameters—a comprehensive sensitivity test was performed, as explained in Table 5. The simulation results from scenarios S2 through S7 are compared with reference to the control scenario (S1) in Fig. 11.

The relative sensitivity reveals that climate change (S3a and S3b) and meteorological forcings (S2a) are the most sensitive factors for flood inundation area and the median flood depths for ME02. Climate change is likely to cause increases of up to 33.7% and 46.5 % in inundated area and median flood depth, respectively. These differences in inundation areas for the aforementioned scenarios can be attributed

mainly to changes in PMP values, revealing that precipitation is the most sensitive factor affecting flood regimes. Reservoir operations (S7) can also contribute moderately by reducing the overall flood inundation area by approximately 13.2 % compared with S1. Note that the reduction is calculated under an ideal reservoir operation scenario and will be directly controlled by the maximum storage capacity of the reservoir. The other two sensitive parameters in this order include the effects of antecedent moisture conditions in the hydrologic model (S6) and the effects of using a high-resolution DEM (S4). They produce relative changes of −8.6% and +6.7%, respectively, for the inundation area. The effect of the Manning's roughness coefficient was found to be the least sensitive factor in this case. A similar trend was also noticed for median flood depths. It should be noted that a minimum depth threshold of 10 cm was utilized to calculate the maximum inundation

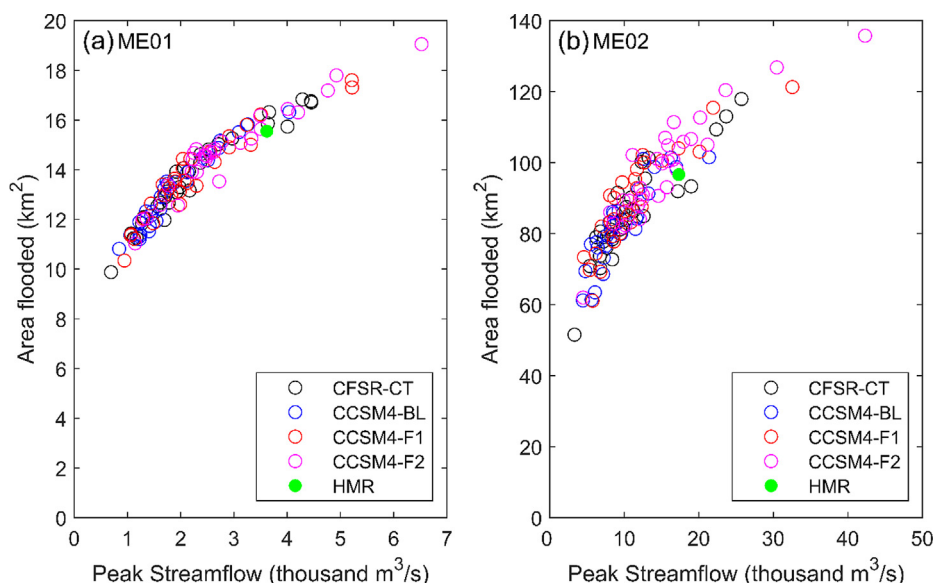


Fig. 8. Flood inundation elasticity with respect to peak discharge for each set of simulations (CFR-CT, CCSM4-BL, CCSM4-F1, and CCSM4-F2) for ME01 and ME02.

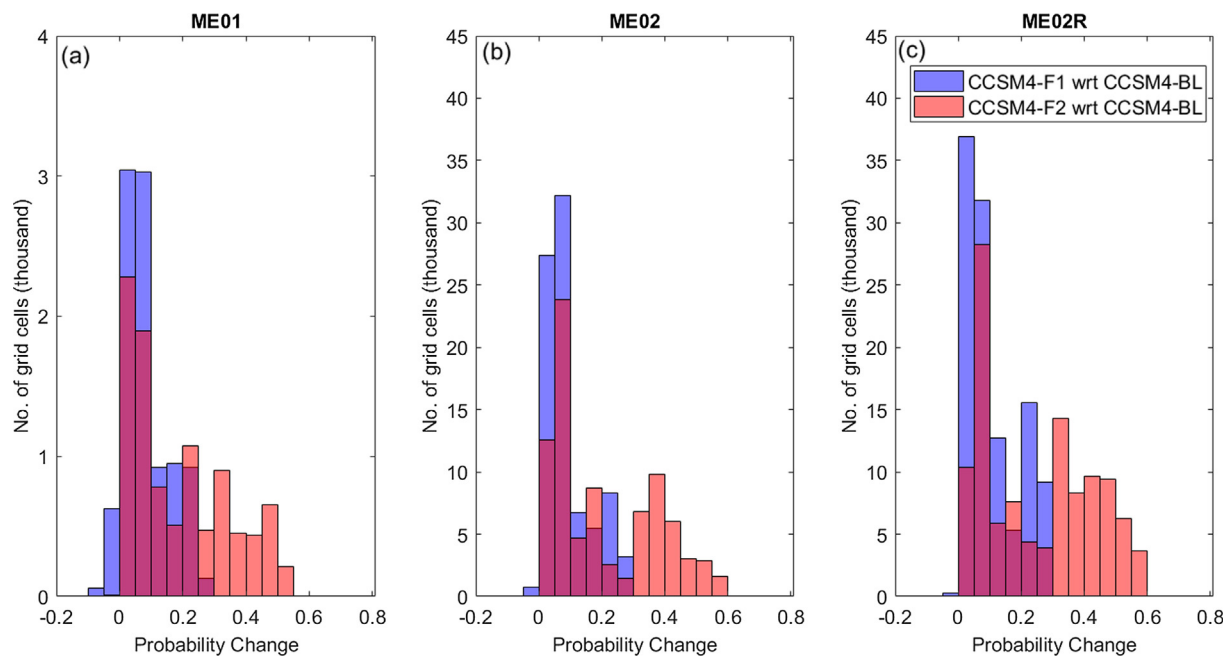


Fig. 9. Changes in flood inundation probability for near future (CCSM4-F1) and far future (CCSM4-F2) periods.

area post-hydrodynamic simulation. We also repeated our analysis using a 1 cm threshold which lead to minimal impacts for our watershed. However, it can have a stronger influence in flat topographies or other regions.

4. Summary and conclusions

This study demonstrates a high-resolution process-based hydro-meteorological modeling framework to generate ensemble-based PFMs for two selected domains for the worst-case flood scenarios (i.e., PMF). An ensemble of 120 moisture maximized PMP storms were acquired

from Rastogi et al. (2017) for historical time period and future climate projections. PMF estimates were then generated by driving DHSVM at a 90-m grid resolution. The 3-hour hydrographs obtained from DHSVM for each storm were used to drive a 2D GPU-accelerated hydraulic model (Flood2D-GPU) at 30-m and 10-m spatial resolutions to produce flood maps for each storm. The probability of inundation was then calculated at each grid cell of the flood domain, which was then used to generate PFMs. Further, the relative sensitivity of flood inundation area and median flood depth was evaluated for various factors such as meteorological forcings, climate change, antecedent moisture conditions, and hydraulic model inputs and parameters.

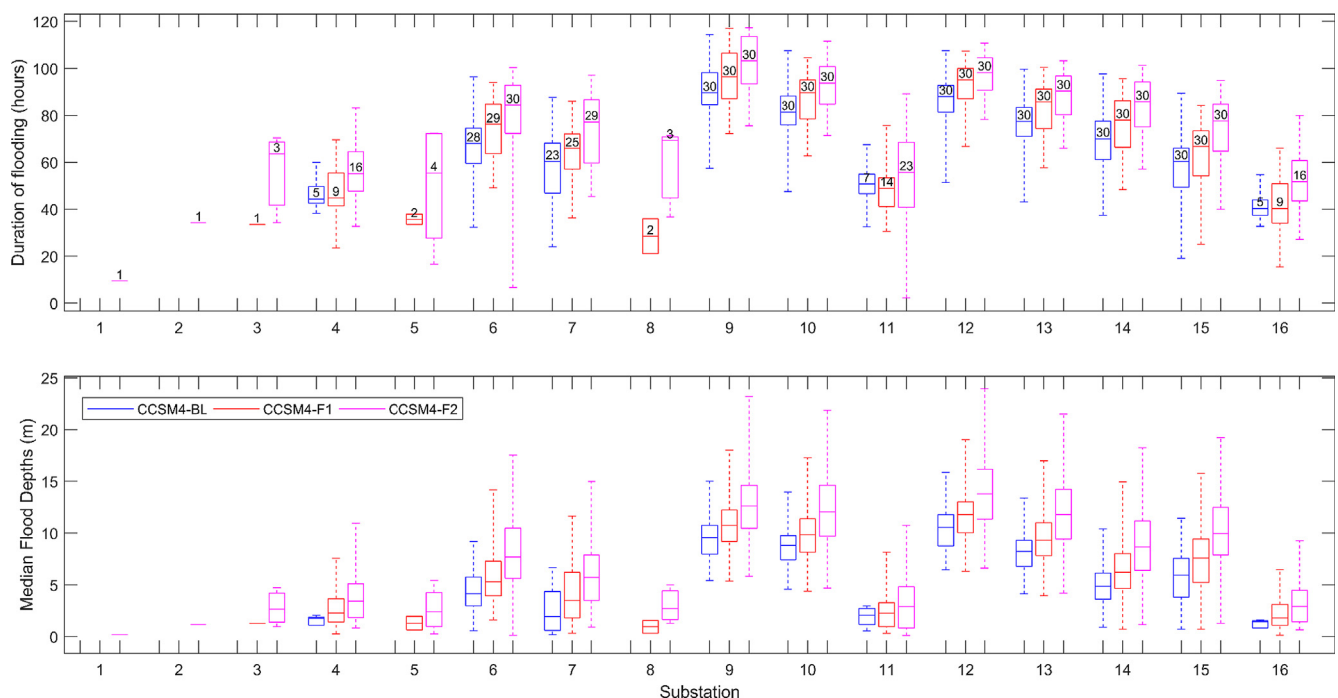


Fig. 10. Flood vulnerability analysis for 16 selected substations for each storm set, i.e. CCSM4-BL, CCSM4-F1, and CCSM4-F2 for ME02. The box plots for duration of flooding and median flood depths are presented in panels a and b, respectively. The number of storms (maximum of 30 storms for each storm set) in which a substation is likely to be flooded is also indicated above the mean of the box plot in Panel a.

Table 5
Scenarios for relative sensitivity test. The Default* setting indicates 30-m for Flood2D-GPU grid resolution and 0.035 as Manning's n value.

Experiment	Scenario ID	Flood2D-GPU Driven by	PMF hydrographs associated with the event with maximum peak discharge (out of 30 events) obtained from CCSM4- forcings (CCSM4- BL)	Flood2D-GPU Resolution	Manning's n
Baseline simulation	S1	PMF hydrographs with maximum peak discharge obtained from CFSR forcings (CFSR-CT)		Default*	Default*
Alternative meteorological forcings	S2a	PMF hydrographs with maximum peak discharge obtained from conventional approach (HMR51 and HMR52)		Default*	Default*
	S2b	PMF hydrographs with maximum peak discharge obtained from near future CCSM4 forcings (CCSM4-F1)		Default*	Default*
Climate change	S3a	PMF hydrographs with maximum peak discharge obtained from far future CCSM4 forcings (CCSM4-F2)		Default*	Default*
	S3b	Same as S1		10-m	Default*
Horizontal grid resolution for Flood2D-GPU	S4	Same as S1		Default*	0.015
Manning's roughness coefficient	S5a	Same as S1		Default*	0.055
	S5b	Same as S1		Default*	Default*
Antecedent moisture conditions	S6	Same as S1, with unsaturated soil moisture conditions at the beginning of hydrologic simulation		Default*	Default*
Reservoir operations	S7	Same as S1, with adjustment to reflect ideal reservoir operations		Default*	Default*

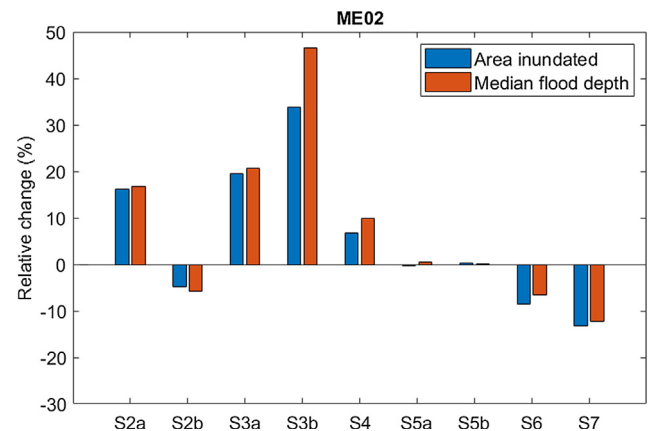


Fig. 11. Figure summarizing the relative sensitivity of area inundated and median flood depths from each scenario with reference to scenario 1 (S1). S2a and S2b are the alternative meteorological forcing scenarios, S3a and S3b are the climate change scenarios, S4 is the varying grid resolution scenario, S5a and S5b are the varying Manning's coefficient scenarios, S6 is the antecedent moisture condition scenario, and S7 is the reservoir operation scenario. Scenario details are provided in Table 5.

The results indicate that the peak discharge from the PMF hydrograph is likely to increase significantly for the Etowah Watershed region under a changing climate. The region downstream of Allatoona Lake is likely to observe an increase of up to 58% in peak discharge magnitude in the near future period (2021–2050, CCSM4-F1), and up to 109% in the far future period (2071–2100, CCSM4-F2) under RCP8.5 compared with the baseline period (1981–2010, CCSM4-CT). These changes in PMF translate into approximately 19% and 33% increases in the flood inundation area. An evaluation of probabilistic inundation maps revealed that the probability of flooding is likely to increase by up to 30% and 60%, respectively, under the near future and far future scenarios. For the 16 selected electrical substations, the vulnerability assessment suggests that over 50% of the selected substations have more than 75% probability of flooding during PMF events in the baseline period. The probability of flooding increases significantly in the projected near and far future periods. For far future scenario CCSM4-F2, all substations are projected to be inundated in at-least one of the ensemble simulations. Additionally, the high-resolution outputs may also provide additional information such as duration of flooding and flood depths under these scenarios.

The relative sensitivity experiments further demonstrated that precipitation is the most sensitive factor affecting the flood regime, including flood inundation areas and depth. The choice of meteorological forcings can contribute to up to a 16% change in the flood inundation area. Further, the flood inundation elasticity relationships developed between peak streamflow and corresponding flood inundation area revealed the uncertainties associated with the shape and timing of hydrographs originating from the spatiotemporal variability in precipitation and the watershed heterogeneity.

The proposed hydro-meteorological modeling framework can enable the generation of probabilistic flood inundation maps through ensemble-based PMP and PMF simulation. The uncertainties associated with the most sensitive factor (i.e., extreme precipitation) and others can be successfully captured with an ensemble approach as presented in this study. The comprehensive relative sensitivity analysis and its effects on flood regime further identify the most important factors causing changes to flood regimes. Although the study focused on a particular HUC08 basin, the framework can be extended to other regions to generate ensemble-based probabilistic flood inundation maps. These maps can serve as an important tool and provide ensemble-based information regarding key flood characteristics (including flood depth and duration) to decision makers, rather than deterministic values

obtained from the conventional approach. Such an evaluation of a region not only determines the regions under flood risk but also informs stakeholders regarding the probability of inundation to enable informed decisions.

Declaration of Competing Interest

None.

Acknowledgments

SG and SCK were supported by the Hydro Research Foundation and US Department of Energy (DOE) Water Power Technologies Office under Award Number DE-00006506. SCK was also partially supported by the U.S. Air Force Numerical Weather Modeling Program. AJK and TTD are supported by the Tennessee Technological University Center for the Management, Utilization and Protection of Water Resources. The research used resources of the Oak Ridge Leadership Computing Facility. Some of the co-authors are employees of UT-Battelle, LLC, under contract DE-AC05-00OR22725 with DOE. Accordingly, the US government retains and the publisher, by accepting the article for publication, acknowledges that the US government retains a non-exclusive, paid-up, irrevocable, worldwide license to publish or reproduce the published form of this manuscript, or allow others to do so, for US Government purposes. The input data sets are cited throughout the paper, as appropriate. The meteorological data was acquired from Rastogi et al. (2017), while the hydrologic model setup was acquired from Gangrade et al. (2018). The open source version of hydrological model (DHSVM) is available at <https://dhsvm.pnnl.gov/code.stm>. Any data questions can be directed to S.-C. Kao (kaos@ornl.gov) at ORNL.

This study was prepared as an account of work sponsored by an agency of the US Government. Neither the US Government nor any agency thereof, nor any of their employees, makes any warranty, express or implied, or assumes any legal liability or responsibility for the accuracy, completeness, or usefulness of any information, apparatus, product, or process disclosed, or represents that its use would not infringe privately owned rights. Reference herein to any specific commercial product, process, or service by trade name, trademark, manufacturer, or otherwise does not necessarily constitute or imply its endorsement, recommendation, or favoring by the US Government or any agency thereof. The views and opinions of authors expressed herein do not necessarily state or reflect those of the US Government or any agency thereof.

References

- Alfieri, L., Salamon, P., Bianchi, A., Neal, J., Bates, P., Feyen, L., 2014. Advances in Pan-European Flood Hazard Mapping. *Hydrol. Process.* 28, 4067–4077. <https://doi.org/10.1002/hyp.9947>.
- Alfonso, B., Mukolwe, M.M., Di Baldassarre, G., 2016. Probabilistic Flood Maps to Support Decision-making: mapping the Value of Information. *Water Resour. Res.* 52 (2), 1026–1043. <https://doi.org/10.1002/2015WR017378>.
- Bates, P.D., De Roo, A.P.J., 2000. A simple raster-based model for flood inundation simulation. *J. Hydrol.* 236 (1–2), 54–77. [https://doi.org/10.1016/S0022-1694\(00\)00278-X](https://doi.org/10.1016/S0022-1694(00)00278-X).
- Beauchamp, J., Leconte, R., Trudel, M., Brissette, F., 2013. Estimation of the Summer-fall PMP and PMF of A Northern Watershed under A Changed Climate. *Water Resour. Res.* 49, 3852–3862. <https://doi.org/10.1002/wrcr.20336>.
- Büchle, B., Kreibich, H., Kron, A., Thieken, A., Ihringer, J., Oberle, P., Merz, B., Nestmann, F., 2006. Flood-risk Mapping: contributions towards an enhanced assessment of extreme events and associated risks. *Nat. Hazards Earth Syst. Sci.* 6, 485–503. <https://doi.org/10.5194/nhess-6-485-2006>.
- Casari, J., Javelle, P., Ramos, M., Leblois, E., 2016. Precipitation ensembles for flood alert. *J. Flood Risk Manage.* 9, 402–415. <https://doi.org/10.1111/jfr3.12203>.
- Daly, C., Halbleib, M., Smith, J.I., Gibson, W.P., Doggett, M.K., Taylor, G.H., Curtis, J., Pasteris, P.P., 2008. Physiographically sensitive mapping of climatological temperature and precipitation across the conterminous United States. *Int. J. Climatol.* 28 (15), 2031–2064. <https://doi.org/10.1002/joc.1688>.
- Di Baldassarre, G., Schumann, G., Bates, P.D., Freer, J.E., Beven, K.J., 2010. Flood-plain Mapping: a critical discussion of deterministic and probabilistic approaches. *Hydrol. Sci. J.* 55 (3), 364–376. <https://doi.org/10.1080/02626661003683389>.
- Domenechetti, A., Vorogushyn, S., Castellari, A., Merz, B., Brath, A., 2013. Probabilistic flood hazard mapping: effects of uncertain boundary conditions. *Hydrol. Earth Syst. Sci.* 17, 3127–3140. <https://doi.org/10.5194/hess-17-3127-2013>.
- FEMA (Federal Emergency Management Agency) (2018), Guidance for Flood Risk Analysis and Mapping; Hydrology: Rainfall-Runoff Analysis, https://www.fema.gov/media-library-data/1520964160255-7c49e1753d0b2634e0c5fb4999459374/Hydrologic_Rainfall_Runoff_Analysis_Feb_2018.pdf, accessed May 2018.
- Fry, J., Xian, G., Jin, S., Dewitz, J., Homer, C., Yang, L., Barnes, C., Herold, N., Wickham, J., 2011. Completion of the 2006 national land cover database for the conterminous United States. *Photogramm. Eng. Remote Sens.* 77 (9), 858–864.
- Gangrade, S., Kao, S.-C., Naz, B.S., Rastogi, D., Ashfaq, M., Singh, N., Preston, B.L., 2018. Sensitivity of probable maximum flood in a changing environment. *Water Resour. Res.* 54 (6), 3913–3936. <https://doi.org/10.1029/2017WR021987>.
- Gent, P.R., Danabasoglu, G., Donner, L.J., Holland, M.M., Hunke, E.C., Jayne, S.R., Lawrence, D.M., Neale, R.B., Rasch, P.J., Vertenstein, M., Worley, P.H., Yang, Z.-L., Zhang, M., 2011. The community climate system model version 4. *J. Climate* 24, 4973–4991. <https://doi.org/10.1175/2011JCLI4083.1>.
- Gesch, D., Oimoen, M., Greenlee, S., Nelson, C., Steuck, M., Tyler, D., 2002. The national elevation dataset. *Photogramm. Eng. Remote Sens.* 68, 5–11.
- Giustarini, L., Hostache, R., Kavetski, D., Chini, M., Corato, G., Schlaffer, S., Matgen, P., 2016. Probabilistic flood mapping using synthetic aperture radar data. *IEEE T. Geosci. Remote Sens.* 54 (12), 6958–6969. <https://doi.org/10.1109/TGRS.2016.2592951>.
- Interagency Advisory Committee on Water Data, 1982. Guidelines for Determining Flood Flow Frequency, Hydrology Subcommittee Bulletin 17B, U.S. Geological Survey, Office of Water Data Coordination, Reston, VA.
- Ishida, K., Kavvas, M., Jang, S., Chen, Z., Ohara, N., Anderson, M., 2015. Physically based estimation of maximum precipitation over three watersheds in Northern California: relative humidity maximization method. *J. Hydrol. Eng.* 20 (10), 04015014. [https://doi.org/10.1061/\(ASCE\)HE.1943-5584.0001175](https://doi.org/10.1061/(ASCE)HE.1943-5584.0001175).
- Jenkins, K., Hall, J., Glenis, V., Kilsby, C., 2017. A probabilistic analysis of surface water flood risk in London. *Risk Anal.* <https://doi.org/10.1111/risa.12930>.
- Kalyanapu, A.J., 2011. Monte Carlo Based Flood Risk Analysis Using a GPU-Enhanced Two-Dimensional Flood Model. Ph.D. dissertation. Department of Civil and Environmental Engineering, University of Utah, Salt Lake City, UT.
- Kalyanapu, A.J., Shankar, S., Pardyjak, E.R., Judi, D.R., Burian, S.J., 2011. Assessment of GPU computational enhancement to a 2D flood model. *Environ. Modell. Softw.* 26 (8), 1009–1016. <https://doi.org/10.1016/j.envsoft.2011.02.014>.
- Kalyanapu, A.J., Judi, D., McPherson, T., Burian, S., 2012. Monte Carlo-based flood modelling framework. *J. Flood Risk Manage.* 5 (1), 37–48. <https://doi.org/10.1111/j.1753-318X.2011.01123.x>.
- Kao, S.-C., DeNeale, S.T., Watson, D.B., 2019. Hurricane harvey highlights: need to assess the adequacy of probable maximum precipitation estimation methods. *J. Hydrol. Eng.* 24 (4), 05019005. [https://doi.org/10.1061/\(ASCE\)HE.1943-5584.0001768](https://doi.org/10.1061/(ASCE)HE.1943-5584.0001768).
- Klein, I.M., Rousseau, A.N., Frigon, A., Freudiger, D., Gagnon, P., 2016. Evaluation of probable maximum snow accumulation: development of a methodology for climate change studies. *J. Hydrol.* 537, 74–85. <https://doi.org/10.1016/j.jhydrol.2016.03.031>.
- Kunkel, K.E., Karl, T.R., Easterling, D.R., Redmond, K., Young, J., Yin, X., Hennon, P., 2013. Probable maximum precipitation and climate change. *Geophys. Res. Lett.* 40, 1402–1408. <https://doi.org/10.1002/grl.50334>.
- Marshall, R., Ghafoor, S., Rogers, M., Kalyanapu, A.J., Dullo, T.T., 2018. Performance evaluation and enhancements of a flood simulator application for heterogeneous HPC environments. *Int. J. Networking Comput.* 8 (2), 387–407.
- McKay, L., Bondelid, T., Dewald, T., Johnston, J., Moore, R., Rea, A., 2012. NHDPlus Version 2: User Guide, available at: ftp://ftp.horizon-systems.com/NHDplus/NHDPlusV2/Documentation/NHDPlusV2_User_Guide.pdf, accessed in August 2017.
- Micovic, Z., Schaefer, M.G., Taylor, G.H., 2015. Uncertainty analysis for probable maximum precipitation estimates. *J. Hydrol.* 521, 360–373. <https://doi.org/10.1016/j.jhydrol.2014.12.033>.
- Miller, D.A., White, R.A., 1998. A conterminous United States multilayer soil characteristics dataset for regional climate and hydrology modeling. *Earth Interact.* 2, 1–26. [https://doi.org/10.1175/1087-3562\(1998\)002<0001:ACUSMS>2.3.CO;2](https://doi.org/10.1175/1087-3562(1998)002<0001:ACUSMS>2.3.CO;2).
- NCEI (National Centers for Environmental Information), 2018. U.S. Billion-Dollar Weather and Climate Disasters, <https://www.ncdc.noaa.gov/billions/>, accessed May 2018.
- Neal, J., Keef, C., Bates, P., Beven, K., Leedal, D., 2013. Probabilistic flood risk mapping including spatial dependence. *Hydrol. Process.* 27 (9), 1349–1363. <https://doi.org/10.1002/hyp.9572>.
- Nuswantoro, R., Diermanse, F., Molkenthin, F., 2016. Probabilistic flood hazard maps for Jakarta. *J. Flood Risk Manage.* 9 (2), 105–124. <https://doi.org/10.1111/jfr3.12114>.
- Ohara, N., Kavvas, M., Kure, S., Chen, Z., Jang, S., Tan, E., 2011. Physically based estimation of maximum precipitation over American River Watershed, California. *J. Hydrol. Eng.* 16 (4), 351–361. [https://doi.org/10.1061/\(ASCE\)HE.1943-5584.0000324](https://doi.org/10.1061/(ASCE)HE.1943-5584.0000324).
- Papaioannou, G., Loukas, A., Vasilades, L., Aronica, G., 2016. Flood inundation mapping sensitivity to riverine spatial resolution and modelling approach. *Nat. Hazards* 83 (Suppl 1), 117–132. <https://doi.org/10.1007/s11069-016-2382-1>.
- Papaioannou, G., Vasilades, L., Loukas, A., Aronica, G.T., 2017. Probabilistic flood inundation mapping at ungauged streams due to roughness coefficient uncertainty in hydraulic modelling. *Adv. Geosci.* 44, 23–34. <https://doi.org/10.5194/adgeo-44-23-2017>.
- Pattison, I., Lane, S.N., Hardy, R.J., Reaney, S.M., 2014. The role of tributary relative timing and sequencing in controlling large floods. *Water Resour. Res.* 50, 5444–5458. <https://doi.org/10.1002/2013WR014067>.
- Pedrozo-Acuña, A., Rodríguez-Rincón, J.P., Arganis-Juárez, M., Domínguez-Mora, R., González Villareal, F.J., 2015. Estimation of probabilistic flood inundation maps for

- an extreme event: Pánuco River, México. *J. Flood Risk Manage.* 8 (2), 177–192. <https://doi.org/10.1111/jfr3.12067>.
- Prasad, R., Hibler, L.F., Coleman, A.M., Ward, D.L., 2011. Design-basis Flood Estimation for Site Characterization at Nuclear Power Plants in the United States of America, PNNL-20091, NUREG/CR-7046. Pacific Northwest National Laboratory, Richland, WA.
- Prime, T., Brown, J.M., Plater, A.J., 2016. Flood inundation uncertainty: the case of a 0.5% annual probability flood event. *Environ. Sci. Policy* 59, 1–9. <https://doi.org/10.1016/j.envsci.2016.01.018>.
- Rastogi, D., Kao, S.-C., Ashfaq, M., Mei, R., Kabela, E.D., Gangrade, S., Naz, B.S., Preston, B.L., Singh, N., Anantharaj, V.G., 2017. Effects of climate change on probable maximum precipitation: a sensitivity study over the Alabama-Coosa-Tallapoosa River Basin. *J. Geophys. Res.* 122, 4808–4828. <https://doi.org/10.1002/2016JD026001>.
- Rousseau, A.N., Klein, I.M., Freudiger, D., Gagnon, P., Frigon, A., Ratté-Fortin, C., 2014. Development of a methodology to evaluate probable maximum precipitation (PMP) under changing climate conditions: application to Southern Quebec, Canada. *J. Hydrol.* 519, 3094–3109. <https://doi.org/10.1016/j.jhydrol.2014.10.053>.
- Saha, S., Moorthi, S., Pan, H.-L., Wu, X., Wang, J., Nadiga, S., Tripp, P., Kistler, R., Woollen, J., Behringer, D., Liu, H., Stokes, D., Grumbine, R., Gayno, G., Wang, J., Hou, Y.-T., Chuang, H.-Y., Juang, H.-M.H., Sela, J., Iredell, M., Treadon, R., Kleist, D., van Delst, P., Keyser, D., Derber, J., Ek, M., Meng, J., Wei, H., Yang, R., Lord, S., van den Dool, H., Kumar, A., Wang, W., Long, C., Chelliah, M., Xue, Y., Huang, B., Schemm, J.-K., Ebisuzaki, W., Lin, R., Xie, P., Chen, M., Zhou, S., Higgins, W., Zou, C.-Z., Liu, Q., Chen, Y., Han, Y., Cucurull, L., Reynolds, R.W., Rutledge, G., Goldberg, M., 2010. The NCEP climate forecast system reanalysis. *B. Am. Meteorol. Soc.* 91, 1015–1057. <https://doi.org/10.1175/2010BAMS3001.1>.
- Schreiner, L.C., Riedel, J.T., 1978. In: Probable Maximum Precipitation Estimates, United States East of the 105th Meridian, Hydrometeorological Report No. 51. National Oceanic and Atmospheric Administration, Washington, D.C., pp. 87.
- Skamarock, W., Klemp, J., Dudhia, J., Gill, D., Barker, D., Duda, M., Huang, X., Wang, W., Powers, J., 2008. A Description of the Advanced Research WRF version 3, NCAR Technical Note, NCAR/TN-475 STR125. National Center for Atmospheric Research, Boulder CO.
- Smemoe, C.M., Nelson, E.J., Zundel, A.K., Miller, A.W., 2007. Demonstrating floodplain uncertainty using flood probability maps. *J. Am. Water Resour. As.* 43 (2), 359–371. <https://doi.org/10.1111/j.1752-1688.2007.00028.x>.
- Storck, P., Bowling, L., Wetherbee, P., Lettenmaier, D.P., 1998. Application of a GIS-based Distributed Hydrology Model for Prediction of Forest Harvest Effects on Peak Stream Flow in the Pacific Northwest. *Hydrol. Process.* 12, 889–904. [https://doi.org/10.1002/\(SICI\)1099-1085\(199805\)12:6<889::AID-HYP661>3.0.CO;2-P](https://doi.org/10.1002/(SICI)1099-1085(199805)12:6<889::AID-HYP661>3.0.CO;2-P).
- Stratz, S.A., Hossain, F., 2014. Probable maximum precipitation in a changing climate: implications for dam design. *J. Hydrol. Eng.* 19 (12), 06014006. [https://doi.org/10.1061/\(ASCE\)HE.1943-5584.0001021](https://doi.org/10.1061/(ASCE)HE.1943-5584.0001021).
- Thornton, P.E., Running, S.W., White, M.A., 1997. Generating surfaces of daily meteorological variables over large regions of complex terrain. *J. Hydrol.* 190, 214–251. [https://doi.org/10.1016/S0022-1694\(96\)03128-9](https://doi.org/10.1016/S0022-1694(96)03128-9).
- USACE (United States Army Corps of Engineers), 1984. HMR52 Probable Maximum Storm (Eastern United States). Hydrologic Engineering Center, Davis, CA.
- Wigmosta, M.S., Vail, L.W., Lettenmaier, D.P., 1994. A distributed hydrology-vegetation model for complex terrain. *Water Resour. Res.* 30 (6), 1665–1679. <https://doi.org/10.1029/94WR00436>.
- Wigmosta, M.S., Nijssen, B., Storck, P., Lettenmaier, D.P., 2002. The distributed hydrology soil vegetation model. In: Singh, V.P., Frevert, D.K. (Eds.), *Mathematical Models of Small Watershed Hydrology and Applications*. Water Resource Publications, Littleton, CO., pp. 7–42.
- Wing, O.E.J., Bates, P.D., Sampson, C.C., Smith, A.M., Johnson, K.A., Erickson, T.A., 2017. Validation of a 30 m Resolution Flood Hazard Model of the Conterminous United States. *Water Resour. Res.* 53, 7968–7986. <https://doi.org/10.1002/2017WR020917>.
- Zischg, A.P., Felder, G., Weingartner, R., Quinn, N., Coxon, G., Neal, J., Freer, J., Bates, P., 2018. Effects of variability in probable maximum precipitation patterns on flood losses. *Hydrol. Earth Syst. Sci.* 22, 2759–2773. <https://doi.org/10.5194/hess-22-2759-2018>.